Voltammetric and Force Spectroscopic Examination of Oxide Formation on Cu(111) in Basic Solution

Myungchan Kang and Andrew A. Gewirth*

Department of Chemistry and Frederick Seitz Materials Research Laboratory, University of Illinois, Urbana, Illinois 61801

Received: April 2, 2002; In Final Form: July 25, 2002

Voltammetry and potential-dependent forces between a Si_3N_4 cantilever and a Cu(111) surface are used to probe the oxidation and reduction of this material in basic solution. In the anodic sweep, potential-dependent adhesive forces obtained from the cathodic limit to the first anodic peak indicate the occurrence of hydroxide adsorption at more negative potentials than the formation of Cu_2O. The reactions through the Cu_2O formation peak are diagnosed as competing scan-rate-dependent reactions that include the oxidation of Cu with both adsorbed OH^- and solution OH^-. The formation of Cu_2O and soluble materials is evident from force measurements. The second anodic peak is associated with a two-electron-transfer reaction along with irreversible reactions producing soluble copper oxide species. The change of adhesive forces in the region of this peak indicates that $Cu(OH)_2$ is formed first and converted to more stable CuO on the surface. Force and scan-rate-dependent voltammetric measurements indicate that the two cathodic peaks correspond to the combination of reduction of soluble and insoluble (adsorbed) copper species. CuOH is a likely intermediate in the final reduction to Cu metal on the cathodic scan. The combination of voltammetry and force spectroscopy provides new insights into the mechanism of the important Cu oxidation process.

I. Introduction

The electrolytic oxidation and reduction of copper surfaces has received considerable attention because of the material's technological importance, especially in processes involving metallization in microelectronic devices.[1−11] Cu oxidation is also an important corrosion reaction in both the acidic and basic environments.

Because of this importance, the formation of passivating layers made of surface oxides in neutral and alkaline solutions has attracted considerable interest in many fields.[12] These studies have sought to elucidate the nature and occurrence of copper surface oxides in aqueous solution. A key issue for which fundamental understanding remains inadequate concerns the electrode potential-dependent formation of adsorbed oxygen and surface oxide species in aqueous media.[10] In particular, there is still uncertainty with regard to the structure of the surface, the potential dependence of this structure, and the presence of any overlayers or adlattices.

Historical studies examining Cu corrosion in basic solutions have focused on voltammetric[11,13−18] and scanning electron microscopy (SEM) measurements.[19,20] Kautek and Gordon[12] used XPS to show that two oxidation states of the oxide grown on Cu were present, depending on the applied potential. The first stage was the formation of Cu_2O, while the second was the formation of $Cu(OH)_2$. Visible light spectroelectrochemical measurements showed that hydroxides of Cu(I) and Cu(II) ware first formed by anodic oxidation at appropriate potentials, and that these then became oxides upon aging.[21] Raman spectroscopy confirmed that a thin Cu_2O film formed as oxidation of the copper surface was initiated. Increasing the potential produced a $Cu(OH)_2$ layer on top of the Cu_2O film. Further oxidation at higher potentials converted the Cu_2O underlayer to $Cu(OH)_2$.[1,10] Other Raman and SEM studies correlated with the voltammetry showed that the formation of Cu_2O occurred at potentials corresponding to the first anodic voltammetric peak, and a porous layer of $Cu(OH)_2$ composed of what appeared in the SEM to be fine needlelike crystals was formed at the second voltammetric peak. The compact underlayer of cuprous oxide was transformed to another species (CuO) upon further oxidation. Reducing this oxide first yields Cu_2O from the underlying CuO film at around 0.1 V vs SHE, followed by $Cu(OH)_2$ reduction to copper, and finally Cu_2O reduction to copper metal.[22] Cu_2O was also observed using in-situ far-infrared spectroscopy.[23]

Ikemiya investigated the structures of aqueous oxide on Cu(111) and Cu(100) in alkaline solutions at pH 13 using in situ atomic force microscopy (AFM) and reported epitaxial Cu_2O structures on both surfaces in the potential range between −0.2 and −0.02 V vs SHE.[6] In situ structural studies[24] using scanning tunneling microscopy (STM) revealed the formation of ordered OH adsorption layers at the initial stage of oxidation and provided images of the formation of the Cu_2O layer.[3] Subsequent oxidation led to a noncrystalline structure.[2−5] X-ray diffraction measurements showed that growth of the oxide occurred primarily at the buried interface between the Cu(111) substrate and the oxide film: the oxide grew inward into the substrate rather than outward into the electrolyte.[9]

Analysis of forces can produce localized chemical information about the sample−liquid interface, such as the nature of surface functional groups or the local effects of the liquid medium.[25−29] In the electrochemical environment, approach curves have been utilized to obtain information about the nature of charge at surfaces in dilute solutions.[28] There have been far fewer potential-dependent adhesion studies. Hudson et al.[30] observed different adhesion forces between neutral and electrochemically

* Author to whom correspondence should be addressed. Phone: 217-333-8329. Fax: 217-333-2685. E-mail: agewirth@uiuc.edu.

10.1021/jp025882y CCC: $22.00
Published on Web 10/29/2002

oxidized polymers. Serafin et al.[31,32] showed the potential dependence of hydrogen bonding adhesive forces between a Si_3N_4 tip and a Au(111) surface in basic solution and a Au(111) surface modified by the underpotential deposition of Bi or Cu in acidic solution.

While the above shows the wealth of information available using structural, voltammetric, and spectroscopic techniques, there are still a number of features of the Cu oxidation and rereduction process in basic solution which need to be examined. In particular, the chemical identity of some of the higher oxidation species and their dynamic behavior are uncertain. In this paper, we revisit the voltammetry of Cu oxide formation on Cu(111) and further use the force-sensing capability of the AFM to probe oxide formation. One advantage of this measurement is the relatively quick (1 s) acquisition time, which is anticipated to be important in a dynamic process such as oxide formation. Force measurements are employed to probe several species of copper oxides (Cu_2O, CuOH, $Cu(OH)_2$, CuO) as a function of the potential in the Cu(111) crystal in basic solution. The change in composition of the surface layers is investigated as a function of applied potential. The results are compared with detailed voltammetric results.

II. Experimental Section

Cu single crystals were (111)-oriented within $\pm 1°$ by using Laue back diffraction. The crystals were mechanically polished with 0.3 μm alumina paste and electropolished in 60% phosphoric acid supersaturated with Cu^{2+} at 1.4 to 1.6 V versus a Cu counter electrode with a current density of 40−60 mA/cm^2 for two minutes.

Voltammetric data were collected using a platinum wire counter electrode and a saturated Ag/AgCl /saturated KCl reference electrode connected to the electrochemical cell via a capillary salt bridge. All potentials reported are relative to SHE. The solutions were purged with Ar prior to use, and a positive pressure of Ar was maintained over the solution in the cell during all electrochemical measurements. Potential control and sweeps were established using a Pine AFRDE-5 potentiostat. Voltammetric data were digitized and collected by computer using a data translation DT-2821 analogue I/O board and software written at the University of Illinois. The electrolyte was prepared from ultrapure NaOH (Aldrich) and Millipore water (resistivity > 18 MΩ cm).

For AFM studies, single crystals were mounted in a small electrochemical cell made of Teflon. The exposed surface area was 0.64 cm^2. The counter and pseudo reference electrodes were both flame-annealed Pt wires. Absolute voltage calibration was achieved by comparing the voltammetry in the AFM cell with voltammetry obtained using a Ag/AgCl reference electrode. Potential control in the AFM cell was maintained with a CV-27 potentiostat (Bioanalytical Systems) using a three-electrode configuration. All linear potential sweep/force measurements used a sweep rate of 1 mV/s. Solutions were deoxygenated prior to use, and the adhesion force measurements were performed under a slight positive pressure of Ar. The electrode surface was prepared by exposing the air-oxidized surface to the electrolyte at open circuit and then scanning the potential from $E = -0.4$ to -1.1 V vs pseudo Pt reference electrode to reduce the oxide film. After this pretreatment, the electrode was scanned to the potential region of interest.

Adhesion measurements were performed in a commercial AFM apparatus (Molecular Imaging), using commercial control and data acquisition electronics (Nanoscope III, Digital Instruments). The probe surface was a commercial Si_3N_4 AFM tip. The surface of the Si_3N_4 is predominately covered by $Si-O^-$ groups under the experimental conditions (pH = 13).[33] The deflection sensitivity of the instrument was calibrated against the linear response in the region of constant compliance, and the scanning piezoelectric crystal was calibrated by imaging a grating of known dimensions. V-shaped cantilevers were used for these experiments, as the spring constants of the torsional modes are large for this geometry.[34]

To reduce piezoelement hysteresis and avoid squeezing action of the tip, we used a scan frequency for force measurements of 0.977 Hz. In JKR theory,[35] work of adhesion is directly related to the force of the adhesion normalized by the radius of curvature of the tip surface[25,36] through

$$W_{ad} = -\frac{2F_{ad}}{3\pi R} \tag{1}$$

where F_{ad} is the force of adhesion, R is the radius of the tip, and W_{ad} is the work of adhesion. To obtain W_{ad}, the radius of the tip is required. The radius of curvature for the probe surface was determined using the procedure of Hütter and Bechhoefer[37] as described previously.[31,32] This procedure relates R to the characteristic "snap-in" distance, d_s, which occurs in the region of mechanical instability when the force gradient of the potential exceeds the spring constant of the cantilever. d_s is read directly off of the force curves. In this procedure,

$$W_{ad} = -\frac{2DA_H}{9\pi d_s^3} \tag{2}$$

where D is the cantilever displacement and A_H is the Hamaker constant for the $Si_3N_4/H_2O/Cu$ system, a quantity that we estimate as equal to 13×10^{-20} J. However, the estimate A_H must of necessity be imprecise (and probably underestimated), especially in the high dielectric strength media used here.[25] The likely underestimation of the Hamaker constant will yield reduced F/R values and hence reduced values for W_{ad}. In this approximation, explicit determination of the cantilever force constant is not required to obtain the work of adhesion. However, some force constants were estimated from the resonance frequency of the cantilever and the manufacturer's specifications of the length and width of the cantilever legs.[38]

III. Results

The Cu(111) system in 0.1 M NaOH was interrogated using voltammetric and force measurements both in approach and retraction.

3.1. Voltammetry. Figure 1 shows cyclic voltammograms (CVs) obtained from a Cu(111) single crystal in 0.1 M NaOH at scan rates of 1 mV/s (Figure 1a) and 20 mV/s (Figure 1b). These two voltammograms show that while some features are scan-rate invariant, others change substantially. The first current peak during the anodic sweep, labeled A1, is due to the oxidation of Cu metal to cuprous oxide, Cu_2O.[1,2,10,11,13,22] The second peak, labeled A2, arises from the oxidation of Cu and Cu_2O to divalent surface and solution-phase species.[1,13] When the sweep is reversed at 1 mV/s, no current is evident as the potential is swept from 0.7 to −0.1 V. A small cathodic peak at −0.25 V (labeled C1) and a large composite cathodic peak (labeled C2a and C2b) are seen over the potential range −0.45 to −0.95 V. These peaks are associated with the reduction of the Cu oxide species and the possible reformation of the bare Cu(111) surface.

At higher scan rates, the voltammetry becomes more complicated. As Figure 1b shows, peak A2 splits into two peaks,

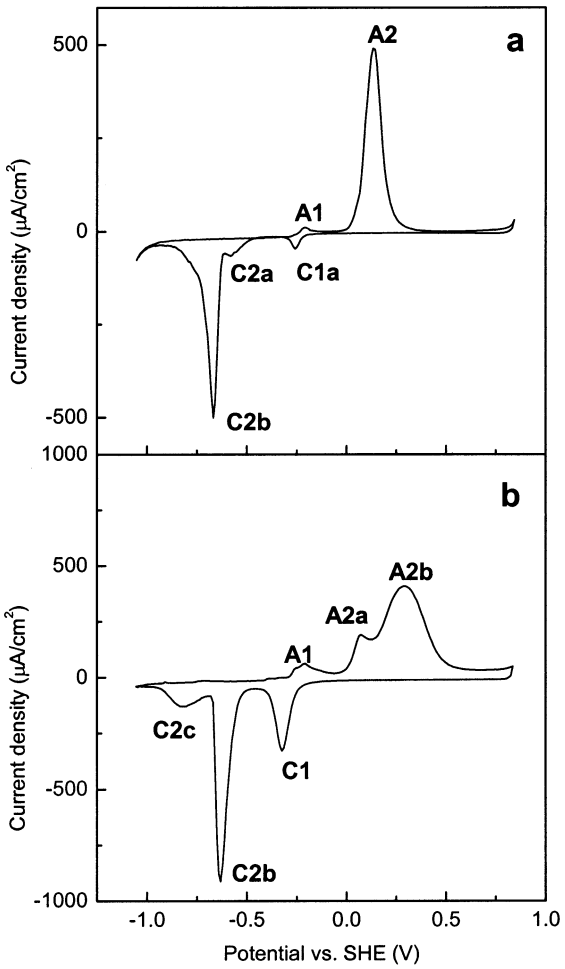

Figure 1. Cyclic voltammograms (CVs) from Cu(111) in 0.1 M NaOH obtained at the scan rate of (a) 1 mV/s and (b) 20 mV/s.

labeled A2a and A2b, at 20 mV/s. On the cathodic sweep, at high scan rate (20 mV/s), the peaks C2a and peak C2b are combined, but the long cathodic tail of C2 visible in Figure 1a separates into two peaks, labeled C2b and C2c. These different features show the time-scale dependence of the reactions on the Cu(111) surface.

3.1.1. Scan-Rate-Dependent Voltammetry. To examine these time scale changes more fully, we performed voltammetric measurements at a variety of different scan rates as shown in Figure 2. To facilitate comparison of voltammetric features, all of the CVs are normalized by dividing the current density by the anodic peak area. Thus, the total anodic peak area for each cyclic voltammogram is unity.

Figure 2a shows a comparison of voltammograms obtained at scan rates between 1 and 20 mV/s. As the scan rate increases, peak A2 starts to divide into A2a and A2b at around a scan rate of 5 mV/s. Interestingly, the width of peak A2a seems scan-rate invariant while that of peak A2b becomes broader, and shifts to more positive potentials as the scan rate increases. In the cathodic sweep, the relative peak area of C1 increases with scan rate. Peak C2a disappears at scan rates higher than 1 mV/s or it may be subsumed in peak C2b. As the scan rate increases, peak C2b splits into two peaks, C2b and C2c. The position and magnitude of peak C2b is scan-rate invariant while peak C2c shifts to negative potentials.

CVs obtained at scan rates between 20 and 50 mV/s are displayed in Figure 2b. As the scan rate increases, peak A2b

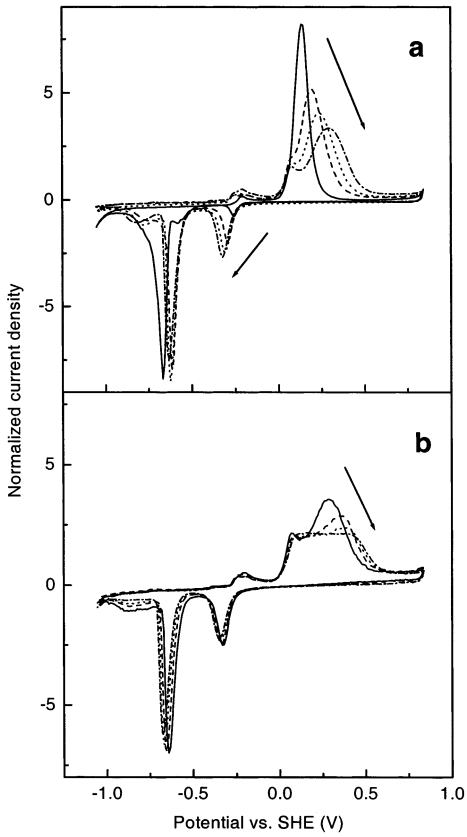

Figure 2. Normalized CVs obtained at a scan rate of (a) (—) 1, (---) 5, (•••) 10, (-•-•) 20 mV/s, and (b) (—) 20, (---) 30, (•••) 40, and (-•-•) 50 mV/s. CVs are normalized by dividing the current density by the anodic peak area. Thus, the total anodic peak area for each CV is unity.

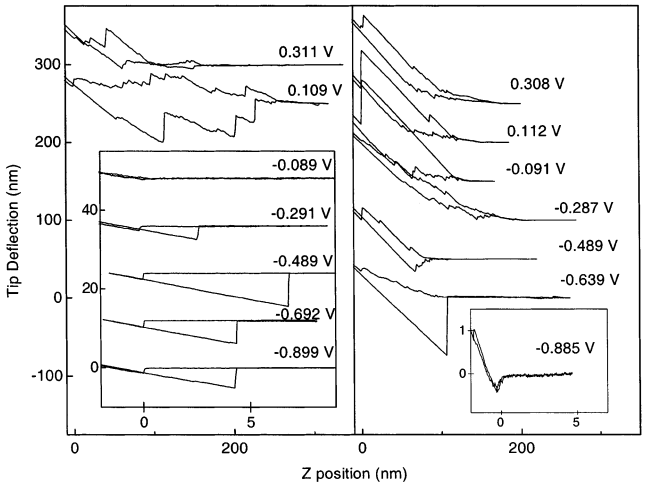

Figure 3. Force curves between a Si_3N_4 tip and Cu(111) in 0.1 M NaOH obtained during anodic (left) and cathodic (right) potential sweeps.

becomes broader, relatively smaller, and shifts to positive potentials. The relative peak areas of C1 and C2b are constant but peak C2c becomes broader and smaller.

No substantive changes in the voltammetry were observed at scan rates higher than 50 mV/s.

3.2. Force Curves. *3.2.1. Anodic Sweep.* Figure 3 shows a series of in situ force curves taken sequentially as the electrode potentials were scanned anodically from −1.0 V up to +0.34 V. The scan was then reversed and further curves were obtained as the potential was swept to negative values. Curves were obtained every 5 s (corresponding to every 5 mV), but only

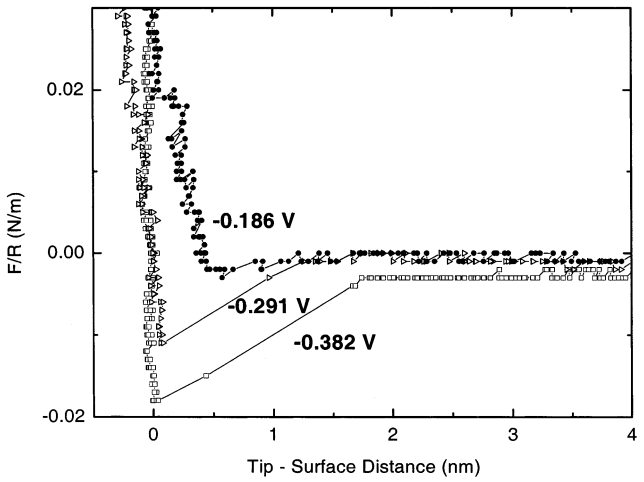

Figure 4. Approach force curves obtained at (open square) −0.382, (rightward open triangle) −0.291, and (solid circle) −0.186 V.

some of the curves are shown in Figure 3. Figure 3 shows that force curve behavior is highly potential dependent. Initially, at negative potentials (shown at the bottom of the first panel), force curves obtained at −0.899, −0.692, and −0.489 V exhibit adhesive behavior on retraction and no repulsive behavior on approach. The jump-to-contact occurs just prior to the region of constant compliance. The lack of repulsive behavior is expected for approach curves obtained above metal surfaces in intermediate molarity electrolyte,[32] as the Debye length is ca. 1 nm in this electrolyte. As the potential becomes more positive and the potential of peak A1 is reached, the force curves exhibit reduced adhesive forces (−0.291 V) and finally no adhesive or repulsive forces (−0.089 V). Force curves with different tips and substrates obtained in this region exhibited a dispersion of ca. 10% in the magnitude of the adhesive interaction.

Interestingly, as shown in Figure 4, the "jump-to-contact" seen at potentials negative of peak A1 disappears as the potential is cycled through this peak. Figure 4 shows that while a substantial jump-to-contact interaction is observed at −0.382 V, this interaction begins to diminish at ca. −0.29 V and has disappeared by −0.19 V. The jump-to-contact interaction remains negligible until the potential of peak A2 is reached.

At the approach to peak A2, the force curves change dramatically. The force curve obtained at 0.109 V exhibits an approach curve that features a sawtooth-like pattern with high repulsion forces extending over several hundred nanometers. The retraction curve features a similar sawtooth-like pattern with high adhesive forces, again stretching over hundreds of nanometers. This behavior is to be contrasted with the ca. 10 nm scale for the adhesive force in the more cathodic region. As the potential is swept to more positive values, the adhesive forces become smaller (0.311 V) and the length scale over which the repulsive forces operate also becomes diminished.

3.2.2. Cathodic Sweep. In the cathodic sweep (right panel of Figure 3), the large length scale of both repulsion and adhesion is maintained until very negative potentials. The sawtooth-like pattern of repulsion remains in evidence until past the potential of peak C1. In the potential region negative of −0.45 V (beginning of peak C2a), the sawtooth-like pattern becomes smoother and the repulsion force becomes smaller, as shown in the force curve obtained at −0.489 V. Around −0.639 V (peak C2b), the repulsion force becomes much smaller, while the adhesive force becomes dramatically larger. Finally, more

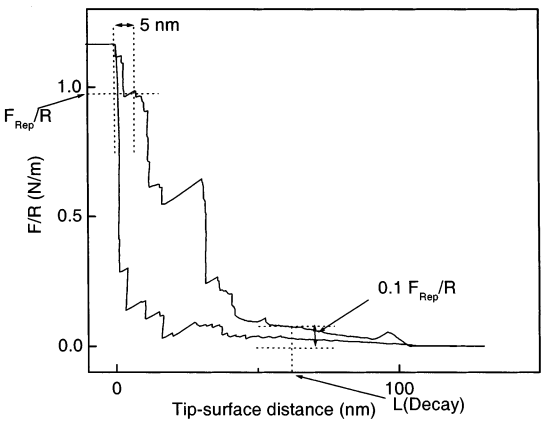

Figure 5. Approach and retraction force curve obtained at 0.320 V.

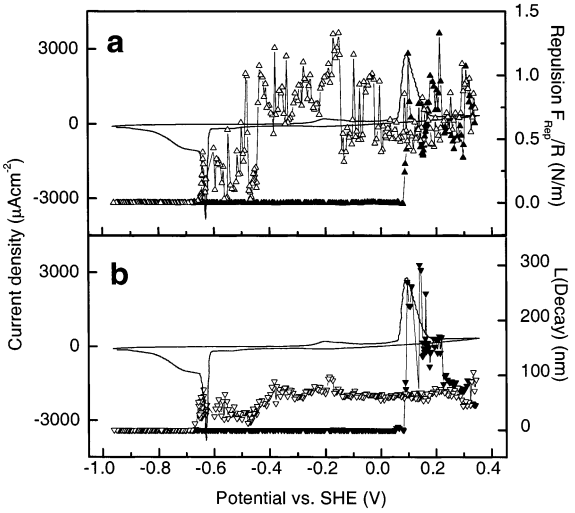

Figure 6. CV obtained in AFM cell and simultaneously measured (a) normalized repulsion force (F_{Rep}/R) and (b) decay length (L_{Decay}) from approach curves. The scan rate is 1 mV/s.

negative of −0.670 V (tail of C2b), the repulsive forces and adhesive force both disappear, as shown in the force curve at −0.885 V.

3.3. Analysis of Force Curves. Figure 5 shows a blow-up of the force curve obtained at 0.320 V on the cathodic sweep. This force curve is used to describe the analysis for subsequent examination. First, for the approach curve, the repulsion force (F_{Rep}/R) is measured 5 nm off of the surface where zero is defined to be the onset of the region of constant compliance. The value of 5 nm is chosen because at these distances the electrostatic force is the main interaction experienced by the tip, as the diffuse charge layers of the two surfaces are still overlapped and generating an attractive or repulsive interaction and the van der Waals interaction is negligible.[39] Second, the decay length (L_{Decay}) is obtained by measuring the tip−surface distance at a value of 1/10 F_{Rep}/R.

For the retraction curves, the minimum point of the curve is used to calculate the adhesive force (F_{Adh}/R). In situations such as that shown in Figure 5 where there is no minimum, the adhesive force is set to zero.

3.3.1. Potential-Dependent Force Information: Approach. Figure 6 shows F_{Rep}/R and L_{Decay} obtained from the approach curves plotted as a function of applied potential. The CV is shown for comparison. The scale of this voltammogram makes peaks C1 and C2a hard to discern, but they can be seen at higher

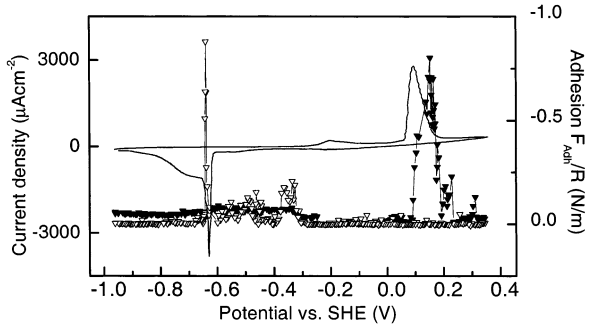

Figure 7. CV obtained in AFM cell and simultaneously measured normalized adhesive force (F_{Adh}/R). The scan rate is 1 mV/s.

magnification. Solid and open symbols in each graph indicate values measured during anodic and cathodic sweeps, respectively.

Figure 6a shows that F_{Rep}/R is negligible below the potential of peak A2. However, at the beginning of peak A2, the repulsion force sharply increases and continues to be large until the potential of peak C2a is reached during the cathodic sweep. The value of F_{Rep}/R appears to increase and become more oscillatory in the potential region around peak C1. Following peak C2a, the repulsion force sharply decreases; in the potential region more negative than peak C2b, the repulsion force disappears.

Figure 6b shows a correlation of decay length with potential. In anodic sweep, the decay length sharply increases to between 150 and 300 nm at the beginning of peak A2 and then gradually decreases to values around 80 nm after passing peak A2. The decay lengths are constant prior to reaching peak C2a during the cathodic sweep. As the potential of peak C2a is passed, the decay length decreases; after passing peak C2b, the decay length decreases to zero.

3.3.2. Potential-Dependent Force Information: Adhesion. Figure 7 shows a graph of the adhesive force obtained as a function of potential. At negative potentials the adhesive force is found to be 0.061 ± 0.012 N/m over a potential range from -1.0 V to -0.350 V. After reaching the potential of peak A1, the adhesive force disappears. The adhesive force sharply increases to a value of ca. 0.80 N/m and then decreases as the potential of peak A2 is passed. As the potential is reversed, the adhesive force returns to zero until reaching the potential of peak C1, where it increases to approximately the value obtained on the anodic sweep although it does appear to fluctuate somewhat. At the potential of peak C2b, very large (ca. 0.9 N/m) adhesive forces are observed. To obtain a clear picture of the potential dependence of this peak, data were obtained every 1 mV in this region. The peak in adhesive interaction occurs some 12 mV after the current peak associated with C2b. After peak C2, the adhesive forces decreases sharply and disappears.

IV. Discussion

The results described above provide considerable insight into processes occurring at or near the Cu(111) surface during oxidation and subsequent rereduction. In what follows, we address each potential region separately and conclude with a unified picture of events at the Cu surface.

4.1. Potential Region Prior to Cu_2O Formation (Lower limit to A1). This potential region features a flat, scan-rate-independent CV, essentially zero repulsion, and decay length. As mentioned, the small repulsion is a consequence of the intermediate electrolyte concentration giving rise to a Debye length of less than 1 nm.[25] The effect of this collapsed double layer has been seen in measurements of repulsive force as a function of electrolyte concentration, which show at intermediate (0.1 M) salt concentrations, that the repulsive component in the force curve has effectively been removed.[40] However, as the electrolyte concentration is increased beyond 0.1 M to 1 M or higher, a repulsive interaction is again observed.[41−43]

This potential region also evinces a constant, nonzero adhesive interaction between the tip and the surface. Previous electrochemical,[11] Raman,[10] and STM[2] work all strongly suggest that the Cu surface at these negative potentials is covered with a monolayer or submonolayer of hydroxide resulting from the underpotential decomposition of water at the Cu surface. The hydroxide coverage on Cu(111) was measured to be ca. $\theta = 0.2$ ML.[4] In addition, most of the reaction pathways already proposed for explaining the copper anodization reaction postulate the electroadsorption of OH^- species on copper active sites as the initial stage.

We now examine the interaction between the tip and a hydroxide-covered surface. The adhesive interaction seen here is due to hydrogen bonding between the surface-bound hydroxide and the $Si-O^-$ groups. We previously examined the interaction of a Si_3N_4 tip with Au(111) in NaOH.[31] In the basic aqueous environment, the probe surface presents primarily $Si-O^-$ functionality, and we interpreted the results to indicate that the variation in the adhesion was primarily due to the interaction of the probe surface with specifically adsorbed OH groups on the surface, with the specific interaction ascribed to hydrogen bonding on the basis of its magnitude.

The measured F_{Adh}/R (force divided by tip radius) in this region is 0.061 ± 0.012 N/m which gives a work of adhesion, $W_{ad} = 12.9 \pm 2.5$ mJ/m^2. With a $Si-O^-$ density of five groups/nm^2,[44] we then get a bond energy of 1.5 kJ/mol. This value is somewhat smaller than that found for the hydrogen-bonding interaction on a AuOH-covered surface (ca. 2 kJ/mol).[31] The discrepancy may possibly be due to the imprecision in determining either the exact $Si-O^-$ coverage on the tip or the effective Hamaker constant. It may also reflect what is likely sparser coverage of OH on the Cu surface in this region relative to the fully covered AuOH surface or another structural issue such as mismatch between the $CuOH_{ads}$ lattice (0.60 nm) and the Si_3N_4 (111) structure (0.48 nm). Finally, the small bond energy may be reflective not of the $Si-O^-{-}HO$ hydrogen bond, but rather the weak $HO-Cu$ physisorption bond.

That the adhesive interaction is present through the entire potential range here strongly suggests that the Cu surface is covered with hydroxide from the most negative potentials until peak A1. We note that the small voltammetric peak at ca. -0.45 V seen by Maurice et al.[4] and associated with hydroxide adsorption was not observed in our work. Droog et al. observed a reversible peak just prior to peak A1, which they associated with hydroxide adsorption on the Cu(111) surface.[17,18] This peak is in evidence in Figure 8 at -336 mV in our work. However, we saw no enhancement in the magnitude of the adhesive interaction going through this peak and therefore cannot assign it to hydroxide association with the Cu surface. We note that Raman measurements report a signal associated with hydroxide throughout the range before peak A1.[10]

4.2. Potential Region between A1 and A2. Peak A1 has been associated with the formation of Cu_2O on the Cu(111) surface. In the potential region between this peak and peak A2, force measurements feature negligible interaction on both approach and retraction. In addition, the jump-to-contact has disappeared. This is in contrast to the more negative region, where a substantial adhesive interaction is measured.

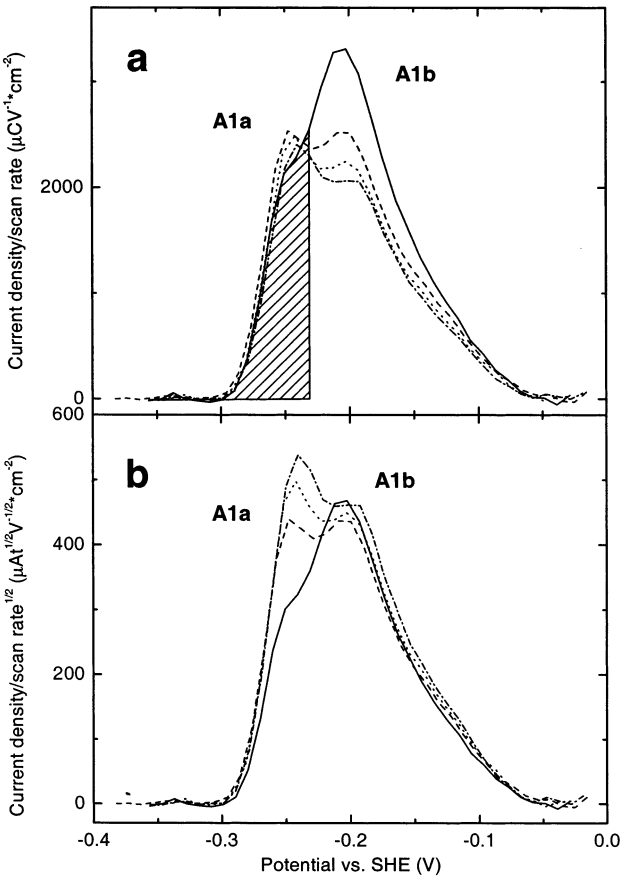

Figure 8. CV obtained in the region around peak A1 at (solid line) 20, (dash line) 30, (dot line) 40, and (dash−dot line) 50 mV/s. The current density of each CV is divided by (a) scan rate and (b) scan rate$^{1/2}$. Each CV has been baseline subtracted. The shaded region is used to approximate the charge passed in peak A1a.

A plethora of measurements show that peak A1 is associated with the oxidation of Cu to yield a multilayer Cu_2O film through the reaction.[1,6,10,22]

$$Cu(0) + OH^- \rightarrow {}^1/_2Cu(I)_2O + {}^1/_2H_2O + e^- \qquad (3)$$

Indeed, the Pourbaix diagram[45] shows that the equilibrium potential for Cu/Cu_2O, $E°(Cu_2O)$, is −0.297 V vs SHE at pH 13. The Cu_2O oxide films are formed with a faceted surface.[3] At higher overpotential, well-crystallized and several-monolayer-thick films are formed and the step edges are not preferential sites of nucleation.[3,9]

The voltammetry shows that there are two sources of the hydroxide required to form the Cu_2O film. Figure 8a shows peak A1 measured at scan rates between 20 and 50 mV/s normalized by the scan rate. Peaks A1a and A1b exhibit different behaviors. Peak A1a is relatively constant when normalized by scan rate, indicating its association with a surface-confined process.[46] The charge approximated for peak A1a in Figure 8a is 63 ± 4 $\mu C/cm^2$. In a one-electron process, this value corresponds to 0.23 ML of copper surface, close to the 0.19 ML hydroxide observed in the STM experiments.[4] Therefore, peak A1a is associated with the reaction of surface hydroxide.

Alternatively, peak A1b is not constant when normalized in this fashion. Figure 8b shows peak A1 normalized by the square root of the scan rate. In this case, peak A1b is constant, which indicates that it is associated with the reaction of materials that are diffusing into the electrode surface.[46] We thus associated peak A1b with diffusion of a species (presumably hydroxide) into the electrode surface. Additional hydroxide would be required to complete the reaction to (a) form multilayers and (b) to compensate for the formation of a soluble species (vide infra).

Because there is no adhesive interaction present in our results, there is likely no hydroxyl species present on the surface in the potential region past peak A1. This indicates that Cu(I)OH and even $Cu(0)-OH_{ads}$ are not the surface species, consistent with previous results. The repulsion at long distances in the approach curve remains negligible for reasons identical with those discussed above.

As shown in Figure 4, the jump-to-contact interaction has disappeared in this region. The jump-to-contact is usually associated with the instability of the tip in the near -surface region as short-range, attractive, van der Waals forces overcome the restoring force of the cantilever.[26,29] The disappearance of this interaction implies that the short-range interactions are now all repulsive or at least not attractive. One reason that short-range interactions can disappear is due to increased solvation in the near-surface region; this is observed to happen in high ionic strength media.[41−43]

We now examine the surface chemistry of the Cu_2O film in order to understand the possible reasons for the disappearance of the short-range attractive force. We associate this disappearance with the appearance of soluble, negatively charged Cu(I) or Cu(II) species which are localized in the near-surface region. The disappearance in the short-range attractive force cannot be due to increasing electrostatic repulsion, as the surface potential here is more positive than that where the jump-to-contact was found. There is considerable precedent in the literature to suggest that soluble Cu(I) or Cu(II) species are formed in the potential region where the Cu_2O film is present. STM studies show step roughening in this region which is associated with slow dissolution of the terraces and a step flow mechanism.[5] Voltammetric[11] and Raman[22] measurements also strongly support the idea of a dissolution process in competition with Cu_2O formation. The soluble Cu material is possibly produced as follows[11,45]

$${}^1/_2Cu(I)_2O + OH^- \leftrightarrow {}^1/_2Cu(I)_2O_2^{2-} + {}^1/_2H_2O \qquad (4)$$

with the subsequent disproportionation of $Cu(I)_2O_2^{2-}$ to CuO_2^{2-}(aq) and Cu(s). Reference to eq 4 shows that an additional hydroxide ion is required to form the soluble material. The requirement for additional hydroxide at the surface should have voltammetric consequences as it implies that additional solution OH^- will be required to diffuse in to complete the reaction forming Cu_2O.

The voltammetry and force spectroscopy thus both point to the existence of a soluble species in the potential range between peaks A1 and A2. This species populates the near-surface region, providing an additional repulsive component in the force curve and effectively shielding the attractive van der Waals interaction between the tip and the sample.

4.3. Potential Region around Peak A2. There are several changes in the force curve as the potential of peak A2 is approached. On the approach side, a strong repulsive interaction is observed starting at 0.1 V and continuing to the anodic limit. The repulsion acts over a long range (ca. 200−300 nm) which is much longer than that expected for a simple electrostatic repulsion arising from the electrochemical double layer (ca. 10−30 nm, depending on electrolyte concentration).[47] In addition, the approach curves feature a sawtooth-like pattern. On the retraction side, the tip−surface interaction becomes quite

adhesive as the potential is swept through peak A2. The adhesive interaction is not simple, as multiple minima are observed.

As the potential is swept past peak A2, the repulsion continues high while the decay length and the adhesive interaction diminish somewhat.

These changes in the force curve cannot be associated with changes in the tip or cantilever, because cycling the potential back to −1.0 V recovers the initial simpler approach and retraction curves. Thus, we look to changes in the Cu surface chemistry to understand the force spectroscopy.

Peak A2 is associated with the oxidation of Cu and Cu_2O to divalent species[1,13] as shown in the following reactions:

$$^1/_2Cu(I)_2O + {}^1/_2H_2O + OH^- \rightarrow Cu(II)(OH)_2 + e^- \quad (5)$$

$$Cu(0) + 2OH^- \rightarrow Cu(II)(OH)_2 + 2e^- \quad (6)$$

$$Cu(II)(OH)_2 \leftrightarrow CuO + H_2O \quad (7)$$

Because the ratio of peaks A2 to A1 is much greater than unity (7:93 at 20 mV/s, 2:98 at 1mV/s), a simple consecutive oxidation of Cu to Cu_2O followed by Cu_2O to CuO or $Cu(OH)_2$ has been rejected[48] and the reaction in eq 6 must dominate that in eq 5. The precise composition of the divalent surface film at the peak A2 (and at more positive potentials) is uncertain, but the most probable divalent surface species are $Cu(OH)_2$, CuO, or a mixed phase of both species.[1]

Complicating the discussion of processes occurring at this peak is the possibility of soluble species at these potentials. Thermodynamic calculations indicate that at least one monovalent and two divalent soluble copper species are expected to be formed in alkaline electrolytes.[49,50] Various divalent copper species are believed to exist, but only the blue cuprite (CuO_2^{2-}) and bicuprite ($HCuO_2^-$) ions predominate at high pH. Solid $Cu(OH)_2$ is considerably more soluble than CuO at pH 13, though CuO is thermodynamically more stable.[22] These compounds are formed through the following reactions:

$$Cu(II)(OH)_2 + OH^- \leftrightarrow HCuO_2^- + H_2O \quad (8)$$

$$Cu(II)(OH)_2 + 2OH^- \leftrightarrow CuO_2^{2-} + 2H_2O \quad (9)$$

Indeed the heterogeneous nature of reactions occurring at peak A2 is evidenced in the voltammetry in Figure 2 where at least two different peaks, A2a and A2b, are observed. Figure 9 shows the CV around A2 measured at scan rates between 5 and 50 mV/s, in which the current density is divided by scan rate. While peak A2a roughly scales with scan rate at higher scan rates, this is not the case for A2b. In addition, the peak potential of peak A2b shifts to positive values with increased scan rate, while that of peak A2a is constant. In the case of peak A1, the peak potential does not shift with scan rate.

The behavior of peak A2 is understood by recourse to the work of Laviron et al.[51] who examined a two-step reversible electrochemical reaction associated with irreversible chemical reactions in thin layer linear potential sweep voltammetry. They used different rate constants of an irreversible reaction with a fixed scan rate, equivalent to the case using different scan rates with a fixed rate constant of an irreversible reaction. Laviron et al. show that for a reaction scheme wherein $O \leftrightarrow P + e^-$ and $P \leftrightarrow R + e^-$ followed by $R \rightarrow Z$ that peak splitting and a progression to positive values of the more anodic peak results with higher scan rate as long as the ratio of equilibrium constants for the first and second reactions is large. At slow scan rates,

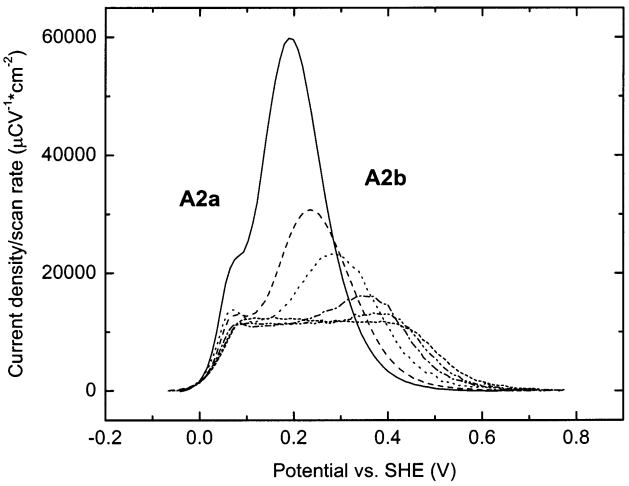

Figure 9. CV obtained in the region around peak A2 at (solid line) 5, (dash line) 10, (dot line) 20, (dash−dot line) 30, (dash−dot−dot line) 40, and (short dashed line) 50 mV/s. The current density of each CV is divided by the scan rate.

only a single peak is observed. This description nicely reproduces the behavior seen in Figure 9.

Applying this result to our system suggests that, eq 6 should be divided to two reactions:

$$Cu(0) + OH^- \rightarrow Cu(I)OH + e^- \quad (6a)$$

$$Cu(I)OH + OH^- \rightarrow Cu(II)(OH)_2 + e^- \quad (6b)$$

and that the $Cu(II)(OH)_2$ decomposes further to soluble species as shown in eq 8 or 9. The behavior of the voltammetry can be understood if the equilibrium constant of eq 6a is much larger than that of eq 6b. This means peak A2a corresponds to the one-electron-transfer reaction oxidizing Cu(0) to CuOH, while peak A2b corresponds to the second electron-transfer reaction followed by irreversible reactions producing soluble copper oxide species.

With this background we now examine the force curves in detail. The high repulsion 5 nm off of the surface starting at peak A2 likely relates to the formation of solvated, charged, soluble species near the electrode surface. The soluble copper oxide ions (CuO_2^{2-} and $HCuO_2^-$) are solvated and intermolecular hydrogen bonding is lost, and in addition there is a change of dielectric constant of the solution near the charged interface. These negative-charged soluble oxide ions produced from the copper surface also would form several layers near the surface at highly positive potentials instead of positive ions. The negatively charged Si_3N_4 tip is repulsed by this negatively charged layer.

In addition to a large repulsive interaction near the surface, this repulsion extends over several hundred nanometers away from the surface during the time the potential is in the region of A2. The high concentration of the soluble species produced in this region, and their necessarily inhomogeneous distribution away from the surface, likely gives rise to the extended repulsion. This idea is consistent with the work of Shoesmith et al.,[52] who suggested that dissolved Cu material forms a supersaturated layer near the surface. The layer remains as long as the potential is held in this region, since dissolution is continuously occurring. The long-range repulsion has also been observed in very highly concentrated electrolytes.[42,43] At the higher concentrations, the double layer turns into an oscillatory ion density profile. The resulting interaction becomes oscillatory,

showing maxima followed by minima as each successive layer is expelled from the gap.[43] Oscillatory forces have been observed by AFM in highly concentrated electrolytes.[53] The sawtooth pattern has also previously been associated with the squeezing of solvent away from the tip and surface over a distance of several nanometers.[54] This provides further support for the idea of an inhomogeneous (and fluxional) distribution of solvated species away from the surface. Finally, we note that the specific shape of the force curve may be a consequence of the fairly high rate of approach (ca. $1-2\ \mu m\ s^{-1}$) used in this study. Long-range repulsion has been observed to increase with approach rate in concentrated solutions.[55]

SEM images obtained from Cu samples immersed in this potential region reveal the presence of Cu oxide needles,[52] and we now evaluate the effect of these on the force curves. One possibility is that the long-range repulsion is associated with the interaction between the tip and these needles. In this model, the tip would impact the needles, breaking them. This impact would be the origin of the rigid contacts (vertical excursions) seen in the approaching force curves. However, this model does not account for the presence of the long range interaction on force curves obtained 1 s apart from each other. For the sawtooth pattern to be observed again, the needles would have to grow to the same extent under the oscillating AFM tip. SPM tips are usually associated with shielding effects which diminish rather than enhance growth. In addition, destructive interactions usually lead to rapid changes in force curve behavior which were not in evidence here. Finally, the sawtooth pattern is observed on retraction, even at potentials where there is no strong adhesion.

As we pass through peak A2, the magnitude of the repulsion 5 nm off of the electrode surface fluctuates, but overall remains high. Alternatively, the decay length drops. This suggests that the amount of soluble species formed has diminished and that the solution several hundred nanometers away from the surface again approaches equilibrium concentrations. Close to the surface, however, the influence of the soluble Cu species remains high.

On retraction, a long-range, multiple minima interaction is again observed. The magnitude of the interaction is also considerably higher than that found at more cathodic potentials. Since high adhesion between a surface and a tip exhibiting $Si-O^-$ groups has previously been associated with hydrogen bonding with surface-confined OH groups,[31,32] we suggest that this interaction is operative here. It is well understood that one of the products of oxidation present on the surface is $Cu(OH)_2$.[1,10,12,22,23] The measured adhesion force is at least an order of magnitude greater in the region around peak A2 (0.05−0.08 N/m vs 0.80 N/m). The coverage of OH in the region negative of peak A1 is only ca. 0.2 ML. In this region, the $Cu(OH)_2$ covers the entire surface and, in addition, presents two OH functionalities per Cu atom. Together, these factors may lead to the increased magnitude of adhesion measured here. Alternatively, the high magnitude of the adhesive interaction and the long range over which it operates strongly suggests that the simple hydrogen bonding between sphere and flat surface (the JKR model) which was used to analyze the more cathodic region is inappropriate. Rather, we suggest that the surface is composed of weakly associated layers of oxidized Cu species, including $Cu(OH)_2$, which are displaced as the tip moves to the region of constant compliance. As the tip is withdrawn, the hydrogen-bonding interaction wraps around the tip and increases both the magnitude and the distance over which it operates. The sawtooth pattern results from the recondensation of the $Cu(OH)_2$ layers back to the surface. Because the interaction is between more than a simple sphere and surface, the JKR analysis which was used to obtain the bond strength is inappropriate.

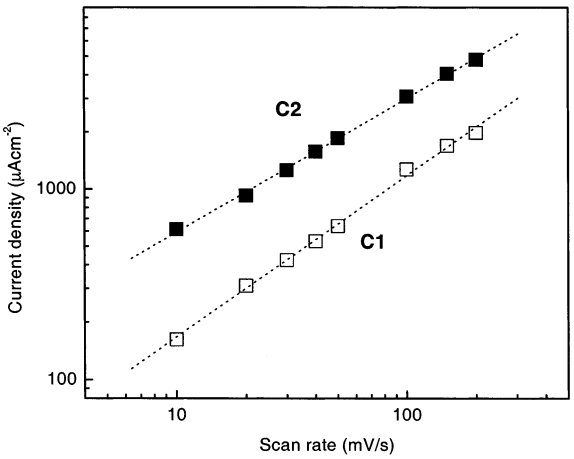

Figure 10. A log−log plot of the current density of peak C1 and C2 obtained at different scan rates vs scan rate.

As the potential is swept past peak A2 to more anodic values, the magnitude of the adhesive interaction decreases. This suggests that the amount of $Cu(OH)_2$ present in the film has diminished. This means that the surface of the film is now CuO, a result confirmed by other measurements.[1,56] CuO is thermodynamically more stable than $Cu(OH)_2$ in this potential region, but its formation may be kinetically limited as the potential passes through peak A2.

4.4. Cathodic Scan: Potential Region around C1 Peak. As the potential sweep is reversed, relatively little change occurs in the force profile until reaching the potential of peak C1. At this potential, the adhesive interaction rises slightly with no change in the repulsive characteristics. As discussed above, an increase in the adhesive interaction is associated with the presence of hydroxide on the surface.

Examining the CV in Figure 2 shows that the relative C1 peak ratio with respect to the anodic charge increases with scan rate. In addition, as shown in Figure 10, current density is proportional to scan rate$^{0.84}$. This indicates the reaction corresponding to peak C1 is the combination of reduction of soluble and adsorbed (insoluble) materials. This is not the case for other peaks, such as A1a, which are associated with surface-confined processes. This means that peak C1 is related to soluble materials, which must diffuse to the surface prior to reduction. The appropriate reactions include reduction of CuO_2^{2-} or $HCuO_2^-$ to solid Cu_2O via

$$2Cu(II)O_2^{2-} + 2e^- + 3H_2O \rightarrow Cu(I)_2O + 6OH^- \quad (10)$$

$$2HCu(II)O_2^- + 2e^- + H_2O \rightarrow Cu(I)_2O + 4OH^- \quad (11)$$

The additional hydroxide present in the near-surface region may lead to the transient formation of the unstable CuOH which would then give rise to the nonzero adhesive interaction observed. We note that CuOH readily converts to Cu_2O in water, and this interconversion may account for the instability in the adhesive interaction in this region. The adhesive interaction observed in the anodic scan was much more stable and reproducible.

The repulsive interaction remains high in this region, suggesting that production of soluble material still occurs. We suggest that the surface is quite heterogeneous in this region and that both Cu_2O and CuO are present. Production of soluble species from CuO or CuO_2 is clearly still an issue here.

4.5. Potential Region around Peak C2. Several things happen as the potential is swept to more negative potentials. As the voltammetry in Figure 2 clearly shows, peak C2 is composed of three different peaks. Peak C2a is broad and small, while peak C2b is sharp and big. Peak C2a is associated with a gradual decrease in the repulsive interaction and the decay length with no change in adhesion. Peak C2b features a sharp, transient rise in the adhesive interaction and a decrease in the repulsive interaction to values associated with the bare metal. As shown in Figure 10, current density is proportion to scan rate$^{0.70}$. This indicates the reaction corresponding to peak C2 is the combination of reduction of soluble and adsorbed (insoluble) materials much in the same way as was the case for peak C1. Finally, as we pass through peak C2a, the repulsion force and decay length both decrease. This means the reaction through C2a is related to the reduction of soluble layers near the surface.

As we pass through peak C2b, the adhesive interaction suddenly increases dramatically and then, at the completion of peak C2b, just as suddenly decreases. Peak C2b is associated with the reduction of CuO and Cu_2O surface and subsurface oxides to Cu metal. The increased adhesion passing through this peak suggests the formation of a hydroxide-containing species on the surface as a possible intermediate to the reduction reaction. A likely candidate is CuOH formed during the one-electron reduction of CuO:

$$\mathrm{Cu(II)O} + \mathrm{H_2O} + \mathrm{e^-} \rightarrow \mathrm{Cu(I)OH} + \mathrm{OH^-} \qquad (12)$$

CuOH is then quickly reduced to Cu(0) or converted to Cu_2O.

Past peak C2b, the repulsive interaction and the decay length all drop to values associated with the metallic Cu surface. The repulsive interaction in this region may be associated with OH^- produced during the reduction process. As this material diffuses into the bulk solution, the repulsive interaction drops. Alternatively, the production of soluble species diffusing away from the surface and giving rise to the ca. 100 nm decay lengths is no longer possible once the CuO and Cu_2O materials have been reduced. As this reduction proceeds, the amount of soluble species drops to zero.

We note that the ratio of anodic to cathodic charge in all of the voltammograms obtained at different scan rates is always greater than unity. This emphasizes the role of soluble oxidized species produced during the Cu(I) and Cu(II) oxide phases, some of which diffuse away from the interface and are never reduced in the cathodic scan.

Finally, there is a residual current tail past peak C2b in the slow scan which evolves to C2c at faster scan rates. Since the interaction of the $Si-O^-$ tip with the surface appears to be unaffected by the processes associated with this current, we suggest that the charge-transfer reaction involved here occurs not on the surface, but rather in the bulk of the Cu material. The delay associated with the tailing current is due to the necessity of water and hydroxide diffusion from the bulk material to the surface which, of necessity, must be slow. Hydrogen evolution occurs at potentials more negative than -1.0 V and is likely not involved in this current at C2c or the corresponding tail to C2b at slower scan rates.

The adhesive interaction in this region is effectively zero, which suggests that hydroxide is not present on the surface. Alternatively, by the time the sweep direction is reversed, the adhesion once again reaches the values reported at the start of the anodic sweep described above. We suggest that the formation of surface hydroxide is a kinetically limited process, and may require the complete reduction of subsurface species. The interplay between these subsurface species and the events surrounding the reformation of the hydroxide adlayer are unknown at present.

V. Conclusion

The analysis presented above shows that the oxidation of Cu(111) in basic solution is a very complex process with scan-rate-dependent reactions competing with those that are surface associated. The force spectroscopy has provided new information about the presence of species presenting OH groups on the surface and their potential-dependent persistence. It also provides information about the production of soluble species that make their presence known through a long-range interaction with the tip. Of particular note is the observation of CuOH as an intermediate in the final reduction to Cu metal on the cathodic scan. We also demonstrate the persistence of a CuOH species over the entire region prior to the formation of Cu_2O on the anodic scan. Finally, the long-range repulsion in evidence from the formation of Cu(II) species on the anodic scan until the final reduction to Cu(0) on the cathodic scan is taken as evidence that soluble species are continually produced in this region.

Acknowledgment. This work was funded by Department of Energy Grant DE-FG02-91ER45349 through the Materials Research Laboratory at the University of Illinois.

References and Notes

(1) Schwartz, D. T.; Muller, R. H. *Surf. Sci.* **1991**, *248*, 349.
(2) Strehblow, H. H.; Maurice, V.; Marcus, P. *Electrochim. Acta* **2001**, *46*, 3755.
(3) Kunze, J.; Maurice, V.; Klein, L. H.; Strehblow, H. H.; Marcus, P. *J. Phys. Chem. B* **2001**, *105*, 4263.
(4) Maurice, V.; Strehblow, H. H.; Marcus, P. *Surf. Sci.* **2000**, *458*, 185.
(5) Maurice, V.; Strehblow, H. H.; Marcus, P. *J. Electrochem. Soc.* **1999**, *146*, 524.
(6) Ikemiya, N.; Kubo, T.; Hara, S. *Surf. Sci.* **1995**, *323*, 81.
(7) LaGraff, J. R.; Gewirth, A. A. *Surf. Sci.* **1995**, *326*, L461.
(8) Cruickshank, B. J.; Sneddon, D. D.; Gewirth, A. A. *Surf. Sci. Lett.* **1993**, *281*, L308.
(9) Chu, Y. S.; Robinson, I. K.; Gewirth, A. A. *J. Chem. Phys.* **1999**, *110*, 5952.
(10) Chan, H. Y. H.; Takoudis, C. G.; Weaver, M. J. *J. Phys. Chem. B* **1999**, *103*, 357.
(11) Gennero De Chialvo, M. R.; Zerbino, J. O.; Marchiano, S. L.; Arvia, A. J. *J. Appl. Electrochem.* **1986**, *16*, 517.
(12) Kautek, W.; Gordon, J. G., II. *J. Electrochem. Soc.* **1990**, *137*, 2672.
(13) Abd El Haleem, S. M.; Ateya, B. G. *J. Electroanal. Chem.* **1981**, *117*, 309.
(14) Ambrose, J.; Barradas, R. G.; Shoesmith, D. W. *J. Electroanal. Chem. Interfacial Electrochem.* **1973**, *47*, 65.
(15) Ambrose, J.; Barradas, R. G.; Shoesmith, D. W. *J. Electroanal. Chem. Interfacial Electrochem.* **1973**, *47*, 47.
(16) Fletcher, S.; Barradas, R. G.; Porter, J. D. *J. Electrochem. Soc.* **1978**, *125*, 1960.
(17) Droog, J. M. M.; Alderliesten, C. A.; Alderliesten, P. T.; Bootsma, G. A. *J. Electroanal. Chem.* **1980**, *111*, 61.
(18) Droog, J. M. M.; Schlentier, B. *J. Electroanal. Chem.* **1980**, *112*, 387.
(19) Shoesmith, D. W.; Rummery, T. E.; Owen, D.; Lee, W. *J. Electrochem. Soc.* **1976**, *123*, 790.
(20) Shoesmith, D. W.; Rummery, T. E.; Owen, D.; Lee, W. *Electrochim. Acta* **1977**, *22*, 1403.
(21) Pyun, C.-H.; Park, S.-M. *J. Electrochem. Soc.* **1986**, *133*, 2024.
(22) Mayer, S. T.; Muller, R. H. *J. Electrochem. Soc.* **1992**, *139*, 426.
(23) Melendres, C. A.; Bowmaker, G. A.; Legar, J. M.; Beden, B. *J. Electroanal. Chem.* **1998**, *449*, 215.
(24) Gewirth, A. A.; Niece, B. K. *Chem. Rev.* **1997**, *97*, 1129.
(25) Israelachvili, J. N. *Intermolecular and Surface Forces*, 2nd ed.; Academic Press: London, 1992.
(26) Cappella, B.; Dietler, G. *Surf. Sci. Rep.* **1999**, *34*, 5.
(27) Carpick, R. W.; Salmeron, M. *Chem. Rev.* **1997**, *97*, 1163.
(28) Takano, H.; Kenseth, J. R.; Wong, S.-S.; O'Brien, J. C.; Porter, M. D. *Chem. Rev.* **1999**, *99*, 2845.
(29) Senden, T. J. *Curr. Opin. Colloid Interface Sci.* **2001**, *6*, 95.
(30) Hudson, J. E.; Abruna, H. D. *J. Am. Chem. Soc.* **1996**, *118*, 6303.

(31) Serafin, J. M.; Gewirth, A. A. *J. Phys. Chem. B* **1997**, *101*, 10833.
(32) Serafin, J. M.; Hsieh, S.-J.; Monahan, J.; Gewirth, A. A. *J. Phys. Chem. B* **1998**, *102*, 10027.
(33) Senden, T. J.; Drummond, C. *J. Colloids Surf. A: Physiochem. Eng. Aspects* **1995**, *95*, 29.
(34) Noy, A.; Frisbie, C. D.; Rozsnyai, L. F.; Wrighton, M. S.; Lieber, C. M. *J. Am. Chem. Soc.* **1995**, *117*, 7945.
(35) Johnson, K. L.; Kendall, K.; Roberts, A. D. *Proc. R. Soc. London, Ser. A* **1971**, *324*, 301.
(36) Drummond, C. J.; Senden, T. J. *Colloids Surf., A* **1994**, *87*, 217.
(37) Hutter, J. L.; Bechhoefer, J. *Rev. Sci. Instrum.* **1993**, *64*, 1868.
(38) Cleveland, J. P.; Manne, S.; Bocek, E.; Hansma, P. K. *Rev. Sci. Instrum.* **1993**, *64*, 403.
(39) Raiteri, R.; Margesin, B.; Grattarola, M. *Sensors Actuators B* **1998**, *46*, 126.
(40) Li, Y. Q.; Tao, N. J.; Garcia, A. A.; Lindsay, S. M. *Langmuir* **1993**, *9*, 637.
(41) Cappella, B.; Baschieri, P.; Frediani, C.; Miccoli, P.; Ascoli, C. *IEEE Eng. Med. Biol.* **1997**, *16*, 58.
(42) Dunstan, D. E. *Langmuir* **1992**, *8*, 740.
(43) Kékicheff, P.; Marčelja, S.; Senden, T. J.; Shubin, V. E. *J. Chem. Phys.* **1993**, *99*, 6098.
(44) Hoh, J. H.; Cleveland, J. P.; Prater, C. B.; Revel, J.-P.; Hansma, P. K. *J. Am. Chem. Soc.* **1992**, *114*, 4917.
(45) Pourbaix, M. *Atlas of Electrochemical Equilibria in Aqueous Solutions*, 2nd ed.; National Association of Corrosion Engineers: Houston, 1974.
(46) Bard, A. J.; Faulkner, L. R. *Electrochemical Methods: Fundamentals and Applications*, 2nd ed.; John Wiley & Sons: New York, 2001.
(47) Hillier, A. C.; Kim, S.; Bard, A. J. *J. Phys. Chem.* **1996**, *100*, 18808.
(48) Macdonald, D. D. *J. Electrochem. Soc.* **1974**, *121*, 651.
(49) De Zoubov, N.; Vanleugenhaghe, C.; Pourbaix, M. *Altas of Electrochemical Equilibria in Aqueous Solutions*; Pergamon Press: New York, 1966; Vol. Sect. 14.1.
(50) Bertocci, U.; Turner, D. R. *Encyclopedia of Electrochemistry of the Elements*; Marcel Dekker: New York, 1974; Vol. 2.
(51) Plichon, V.; Laviron, E. *J. Electroanal. Chem.* **1976**, *71*, 143.
(52) Shoesmith, D. W.; Rummery, D.; Owen, D.; Lee, W. *J. Electrochem. Soc.* **1976**, *123*, 790.
(53) Fielden, M. L.; Hayes, R. A.; Ralston, J. *Phys. Chem. Chem. Phys.* **2000**, *2*, 2623.
(54) O'Shea, S. J.; Welland, M. E.; Rayment, T. *Appl. Phys. Lett.* **1992**, *60*, 2356.
(55) Addai-Mensah, J.; Dawe, J.; Hayes, R.; Prestidge, C.; Ralston, J. *J. Colloid Interface Sci.* **1998**, *203*, 115.
(56) Strehblow, H.-H.; Titze, B. *Electrochim. Acta* **1980**, *25*, 839.